

# GSTO: Gated Scale-Transfer Operation for Multi-Scale Feature Learning in Pixel Labeling

Zhuoying Wang<sup>1</sup>, Yongtao Wang<sup>1\*</sup>, Zhi Tang<sup>1</sup>,  
Yangyan Li<sup>2</sup>, Ying Chen<sup>2</sup>, Haibin Ling<sup>3</sup>, Weisi Lin<sup>4</sup>

<sup>1</sup>Peking University, <sup>2</sup>Alibaba Group

<sup>3</sup>Stony Brook University, <sup>4</sup>Nanyang Technological University

{wzypku, wyt, tangzhi}@pku.edu.cn, {chenying.aialab, yangyan.lyy}@alibaba-inc.com  
hling@cs.stonybrook.edu, wslin@ntu.edu.sg

## Abstract

*Existing CNN-based methods for pixel labeling heavily depend on multi-scale features to meet the requirements of both semantic comprehension and detail preservation. State-of-the-art pixel labeling neural networks widely exploit conventional scale-transfer operations, i.e., up-sampling and down-sampling to learn multi-scale features. In this work, we find that these operations lead to scale-confused features and suboptimal performance because they are spatial-invariant and directly transit all feature information cross scales without spatial selection. To address this issue, we propose the Gated Scale-Transfer Operation (GSTO) to properly transit spatial-filtered features to another scale. Specifically, GSTO can work either with or without extra supervision. Unsupervised GSTO is learned from the feature itself while the supervised one is guided by the supervised probability matrix. Both forms of GSTO are lightweight and plug-and-play, which can be flexibly integrated into networks or modules for learning better multi-scale features. In particular, by plugging GSTO into HRNet, we get a more powerful backbone (namely GSTO-HRNet) for pixel labeling, and it achieves new state-of-the-art results on the COCO benchmark for human pose estimation and other benchmarks for semantic segmentation including Cityscapes, LIP and Pascal Context, with negligible extra computational cost. Moreover, experiment results demonstrate that GSTO can also significantly boost the performance of multi-scale feature aggregation modules like PPM and ASPP. Code will be made available at <https://github.com/VDIGPKU/GSTO>.*

## 1. Introduction

Pixel labeling tasks, such as semantic segmentation and human pose estimation, target at assigning contextual labels for each pixel of an image, and are requested to deal with classification and localization simultaneously [35]. Since classification requires a large receptive field for inferring the semantic category while localization requires high-resolution details for outlining the precise boundary, how to meet both the requirements is essential for the design of dense-pixel labeling algorithms [3].

Current state-of-the-art pixel-labeling methods generally exploit multi-scale features to handle the aforementioned issue and have obtained impressive results. Ideally, multi-scale features work by assigning pixels to a proper receptive field according to its positions and object scales, but in practice the learned features are often scale-confused. An example is shown in Figure 1(a), where the multi-scale features are extracted from an image of Cityscapes val dataset by HRNetV2-W48 [40], one of the most powerful backbones for semantic segmentation. One can observe that, in general, on the high-resolution feature map with small receptive field, small objects (e.g., person and traffic light) and the boundaries of large objects are highlighted, while on the low-resolution feature map with large receptive field, larger objects like car and road are stressed. Such observations show that the learned multi-scale features are mainly scale-aware, that is, the high-resolution features are responsible for sensing small objects and boundaries, while the low-resolution features are concerned with large objects. However, if investigating more carefully, we can find that the features learned by HRNetV2-W48 are not sufficiently scale-aware, that is, some parts of large objects incorrectly fire high activation responses on the high-resolution features and large objects are insufficiently focused on the low-resolution features.

In this work, for the first time, we show that such scale-

\*Corresponding author

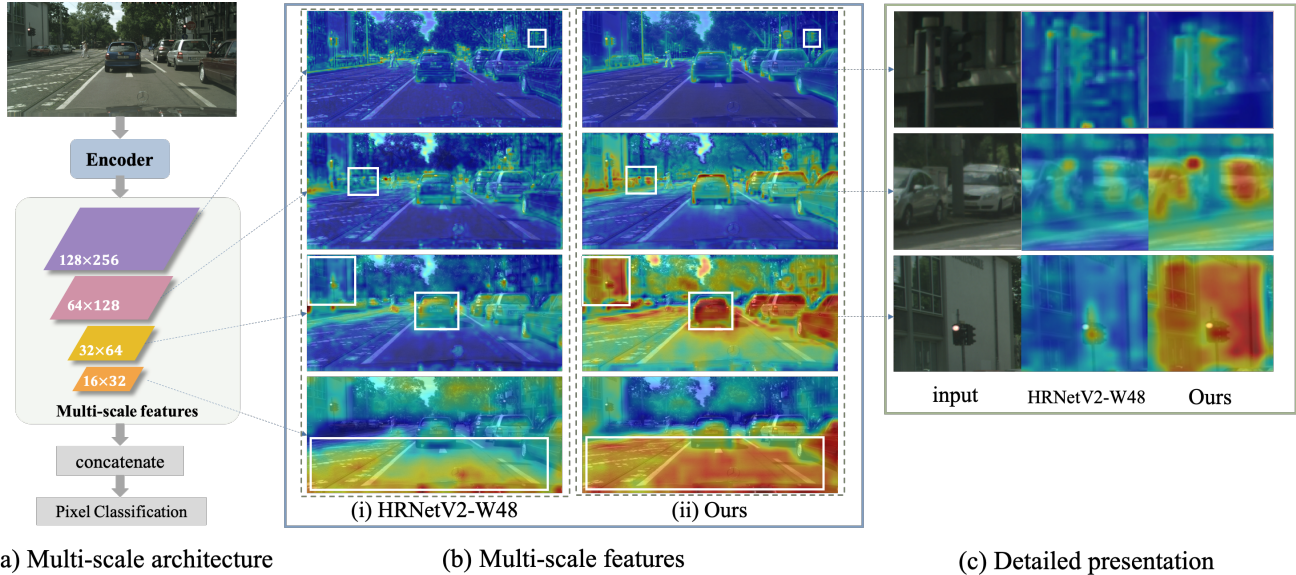


Figure 1: Visual comparison of the multi-scale features extracted by the encoder of (i) HRNetV2-W48 and (ii) our proposed GSTO-HRNet. Each heat map is obtained by averaging the corresponding feature map along the channel dimension, and warmer color (red) indicates larger activation. The comparison demonstrates that our approach obtains more discriminate and scale-aware features, where small objects like “traffic light and object boundaries are more precisely highlighted in the high-resolution feature map, while medium-size objects like car and far-away building as well as large objects like road and nearby car are better focused in low-resolution feature maps. On the contrast, HRNetV2 suffers from feature-confusion, that is, some parts of large objects incorrectly fire high activation responses on the high-resolution features and large objects are insufficiently focused on the low-resolution features.

confusion is attributed to the spatial-invariant scale-transfer operations (i.e., up-sampling and down-sampling) that are extensively exploited by existing pixel labeling methods when learning multi-scale features. These operations directly transit all feature information cross scales without scale-aware selection, leading to suboptimal performance.

To alleviate the above scale-confusion and learn scale-aware features for pixel labeling, we propose novel Gated Scale-Transfer Operations (GSTO) of two forms, unsupervised GSTO and supervised GSTO, to properly transit a feature map across scale. Specifically, unsupervised GSTO directly produces a pixel-wise gating map from the feature map itself, while supervised GSTO learns the gating map with supervision during the training phase. The proposed two GSTOs are lightweight and plug-and-play, thus it can be flexibly integrated into networks or modules for learning better multi-scale features at only minor extra computation cost. By replacing conventional scale-transfer operation with the proposed GSTO in HRNet [39, 40], our approach, denoted as GSTO-HRNet, enjoys much more discriminative features for each scale. As shown in Figure 1(b), object boundary is more precisely outlined on high-resolution feature maps, and large objects are better focused on low-resolution feature maps. Quantitatively,

GSTO-HRNet achieves new state-of-the-art results for human pose estimation on the COCO dataset with only a half amount of parameters and FLOPs, and for semantic segmentation on the Cityscapes, LIP and Pascal Context datasets with negligible extra computational costs. Extensive results show that the proposed GSTO can also improve modules for multi-scale feature aggregation modules like Pyramid Pooling Module [52] and Atrous Spatial Pyramid Pooling Module [4] by a large margin.

In summary, our contributions are three-fold:

- We propose two novel light-weight Gated Scale-Transfer Operations (GSTOs), unsupervised GSTO and supervised GSTO, to learn better multi-scale features for pixel labeling.
- By plugging GSTOs into HRNet, we further propose a backbone named GSTO-HRNet and achieve new state-of-the-art results on multiple benchmarks for both semantic segmentation and human pose estimation.
- The proposed GSTOs can also significantly improve the performance of modules for multi-scale feature aggregation modules.

## 2. Related Work

### 2.1. Pixel labeling networks

Pixel labeling tasks like semantic image segmentation and human pose estimation, require the capturing of both high-level semantic category and low-level spatial details. Though current CNN-based methods [36, 2, 23] reduce down-sampling layers to keep high-resolution [36] and exploit dilated convolution [5] as well as large-kernel [35] convolution to expand the receptive field, multi-scale feature exploiting is still the most effective way to handle the above problem. Multi-scale aggregation modules [52, 4, 47] are introduced at the end of encoder to extract features of various receptive fields. Multi-stage networks [30, 9] are further exploited to processively combine semantic information and spatial details. Recently, an efficient and powerful backbone HRNet [39, 40] is proposed to process multi-scale features in parallel, reaching the best results on multi-ple benchmarks.

### 2.2. Scale-transfer Operations

Conventional scale-transfer operations like average pooling and bilinear interpolation are widely used as cross-scale transition methods in current multi-scale feature aggregation modules [5, 52, 47, 42] and multi-scale feature extraction backbones [39, 40] for pixel labeling tasks. Besides, a few other transfer operations have been proposed. For example, [38] proposes an efficient sub-pixel convolution layer to learn an array of upscaling filters and up-scale the low-resolution features. [43] introduces a data-dependent up-sampling method to replace the bilinear in decoders for semantic segmentation. Generally speaking, all of the aforementioned methods are designed only for upscaling, not plug-and-play, and suffer from heavy computational costs.

### 2.3. Gate Mechanism

Gate mechanism has been widely exploited in computer vision to enhance the representational power by modeling channel-wise or spatial-wise relationship. [44, 34, 17, 45] In pixel labeling tasks, self-attention mechanism is proposed to use the weighted combination of pixels or channels as the context. [6] designs a network to learn gates to ensemble multi-scale results at the end of model. Gated-SCNN[42] proposed a two-stream CNN architecture and utilize gate mechanism to wire shape information as a separate processing branch. Inspired by the works above but different, we argue that *inserting heavy attention modules after each block or the whole backbone brings limited improvement*, and we further propose a light-weight gate mechanism and equip it with scale-transfer operations, significantly improving the performance of multiple multi-scale feature extraction methods.

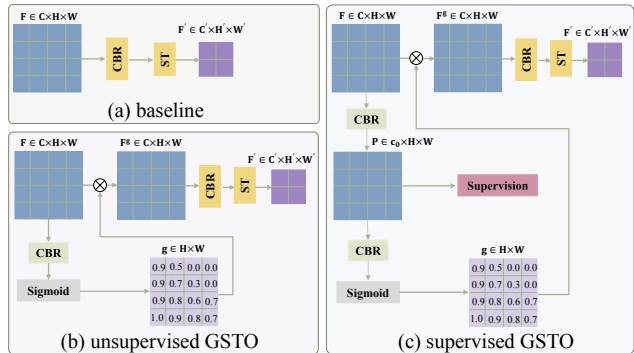


Figure 2: Structures of the proposed unsupervised GSTO and supervised GSTO. **CBR** represents Conv+BN+ReLU, used to change the channel size, if needed, and **ST** refers to conventional scale-transfer operation including down-sampling and up-sampling.

## 3. Method

In this section, we first introduce the principle of our proposed Gated Scale-Transfer Operation (GSTO) and its two forms in Section 3.1. Then we illustrate how to equip multi-scale backbones with GSTO and describe the pipeline of the advanced backbone GSTO-HRNet in Section 3.2. Lastly in Section 3.3, we show how to improve general multi-scale feature aggregation modules by utilizing GSTO with an example.

### 3.1. Gated Scale-Transfer Operation

The intuition of Gated Scale-Transfer Operation is to learn a spatial mask that filters pixels inconsistent with the target scale. The operation works during the cross-scale feature transition. We denote the initial feature to be transited as  $F \in \mathbb{R}^{C \times H \times W}$ , with  $C$  channels of size  $(W, H)$ , and the target feature as  $F' \in \mathbb{R}^{C' \times H' \times W'}$ , with  $C'$  channels of size  $(W', H')$ . The feature vector at location  $(i, j)$  ( $i = 1, \dots, H$ ,  $j = 1, \dots, W$ ) is denoted as  $F_{ij} \in \mathbb{R}^C$ , and similar notation is used for  $F'$ .

#### 3.1.1 Traditional Scale-Transfer Operation

As shown in Figure 2(a), traditional transition is performed through down-sampling like average pooling and up-sampling like bilinear interpolation. Additionally, if  $C \neq C'$ , convolutional layers are needed for channel modification. The process can be represented as follows:

$$\tilde{F}_{kij} = \sum_{m=1}^C \omega_{km} \cdot F_{mij}, \quad k = 1, \dots, C', \quad (1)$$

$$F' = ST(\tilde{F}), \quad (2)$$

where  $\tilde{F} \in \mathbb{R}^{C' \times H \times W}$  is computed by a  $1 \times 1$  convolution,  $\omega_k \in \mathbb{R}^C$  is the  $k$ -th convolutional kernel, and  $ST$  repre-

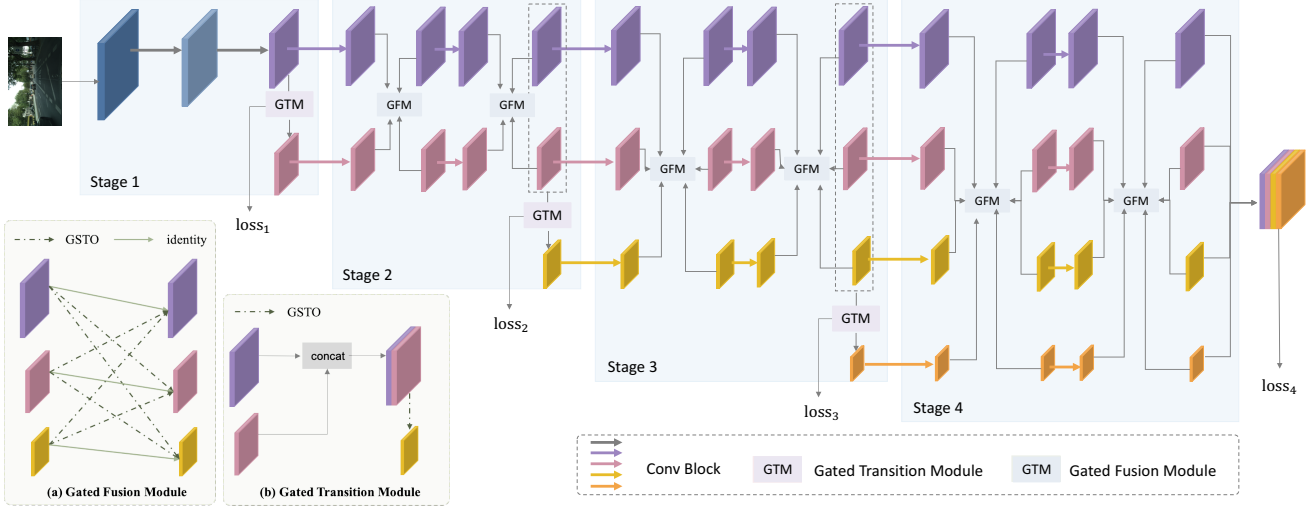


Figure 3: The pipeline of GSTO-HRNet, the GSTO-advanced multi-scale backbone(described in Section 3.2). The GFM and GTM are GSTO-based modules for multi-scale feature fusion and generation, respectively.

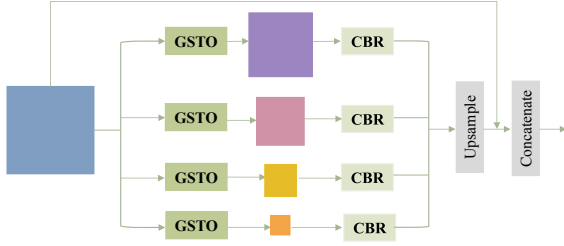


Figure 4: GSTO-based Pyramid Pooling Module: an example to advance multi-scale aggregation modules with the proposed GSTO. **CBR** represents Conv+BN+ReLU.

sents traditional scale-transfer operations.

### 3.1.2 Gated Scale-Transfer Operation

In the proposed GSTOs (Figure 2(b) and (c)), a spatially gated feature  $F^g$  is produced firstly and then Equations 1 and 2 are performed on  $F^g$  instead of on the original  $F$ . The element of  $F^g$  is calculated by element-wise multiplication as follows:

$$F_{mij}^g = g_{ij} \cdot F_{mij}, \quad m = 1, \dots, C, \quad (3)$$

where  $g_{ij} \in \mathbb{R}$  is the corresponding value of the gate at location  $(i, j)$ .

For **unsupervised GSTO** (see Figure 2(b)), element of the gate  $g_{ij}$  is calculated from the original feature  $F$ , by an  $1 \times 1$  convolution with input channel of  $C$  and output channel of 1, followed by sigmoid, which can be denoted as:

$$g_{ij} = \sigma\left(\sum_{m=1}^C \rho_m \cdot F_{mij}\right), \quad (4)$$

where  $\rho \in \mathbb{R}^C$  is the weight of the convolution, and  $\sigma(\cdot)$  is the *sigmoid* function defined as  $\sigma(x) = (1 + e^{-x})^{-1}$ .

As for **supervised GSTO** (see Figure 2(c)), a light-weight predictor, such as a  $1 \times 1$  convolution, is performed on  $F$  to get  $P \in \mathbb{R}^{c_0 \times H \times W}$ , where  $c_0$  is the number of semantic categories and  $P$  is supervised by the ground truth during training process.  $P_{nij}$  measures the probability that pixel  $(i, j)$  belongs to the  $n$ -th class. Then we apply a  $1 \times 1$  convolution on  $P$  to get the spatial mask. The process is represented mathematically as follows:

$$P_{nij} = \sum_{m=1}^C \omega'_{nm} \cdot F_{mij}, \quad n = 1, \dots, c_0, \quad (5)$$

$$g_{ij} = \sigma\left(\sum_{n=1}^{c_0} \theta_n \cdot P_{nij}\right), \quad (6)$$

that is to say, each element of the learned  $\theta \in \mathbb{R}^{c_0}$  corresponds to a semantic category and represents the weight of this category when transferred to the target scale.

## 3.2. Multi-scale Backbone with GSTO

The recently proposed multi-scale backbone HRNet [40, 39] has shown impressive results in pixel labeling. With our proposed GSTO, we build an advanced backbone named GSTO-HRNet (the pipeline is shown in Figure 3). We focus on the multi-scale feature fusion after each block and the lower-resolution branch generation after each stage, and introduce corresponding GSTO-based modules: Gated Fusion Module (GFM) and Gated Transition Module (GTM).

Method	mIoU
baseline [40]	75.9( <i>impl</i> )
baseline(w/ sup)	76.3(0.4 ↑)
baseline+GFM	76.6(0.7 ↑)
baseline+GTM(w/o sup)	76.4(0.5 ↑)
baseline+GTM(w/ sup)	77.0(1.1 ↑)
baseline+GTM(w/o sup)+GFM	76.8(0.9 ↑)
baseline+GTM(w/ sup)+GFM	<b>77.2</b> (1.3 ↑)

Table 1: Comparison experiments of GFM and GTM.

### 3.2.1 Gated Fusion Module

In the design of GFM (Figure 3(a)), we follow the densely-connected pattern in HRNet [39] but replace the traditional cross-scale interaction with the proposed Gated Scale-Transfer Operation. Since GFM is performed after every block, we exploit unsupervised GSTO for efficiency.

### 3.2.2 Gated Transition Module

Lower-resolution represents larger receptive field. HRNet cuts down the feature resolution by half after each stage through a  $3 \times 3$  stride convolution layer performed on the current lowest-resolution feature map. But for dense-pixel tasks, we prefer to keep the pixels that have been semantically comprehended in the high-resolution branch while transit those requiring larger receptive field to the lower resolution one. So we adopt GSTO to achieve the selection. In the proposed Gated Transition Module (Figure 3(b)), we up-sample the features from each branch to the same resolution and concatenate them along the channel dimension. Then GSTO is performed on the united feature to get a lower-resolution branch. We will experimentally compare the unsupervised GSTO and supervised GSTO in Section 4.4. When we use supervised GSTO, the final loss is set as  $0.2 \times loss_1 + 0.3 \times loss_2 + 0.5 \times loss_3 + 1.0 \times loss_4$ , where  $loss_i$  is the cross-entropy loss of the  $i$ -th stage.

### 3.3. Multi-scale Modules with GSTO

Besides the above mentioned multi-scale backbones, traditional classification backbone can gain improvement by applying GSTO to multi-scale aggregation modules like Pyramid Pooling Module (PPM) [52] and Atrous Spatial Pyramid Pooling (ASPP) [4]. Figure 4 shows an example of PPM advanced by GSTO. Generally, GSTO can be adopted to replace the conventional scale-transfer operations as adaptive pooling or atrous convolution to expand the receptive field.

Stage1	Stage2	Stage3	#Param.	GFLOPs	mIoU
✗	✗	✗	3.93M	71.7	76.6
✗	✗	✓	3.95M	73.9	76.7
✗	✓	✓	3.95M	74.4	<b>77.3</b>
✓	✓	✓	4.02M	83.0	77.2

Table 2: Ablation study for the number of GTM. The base model is HRNetV2 with GFM only(the first row).

Attention form	Location	#Param.	GFLOPs	mIoU
channel-wise	after each block	3.93M	71.6	75.9
spatial-wise	after each block	3.92M	71.7	76.2
channel-wise	after each layer	3.94M	71.6	76.1
spatial-wise	after each layer	3.93M	72.1	76.4
channel-wise	combined with ST	3.94	71.6	76.2
spatial-wise	combined with ST	3.93M	71.7	<b>76.8</b>

Table 3: Comparison of different gating/attention mechanism. ST means Scale-transfer operation. All the experiments are conducted without extra supervision.

Method	Backbone	#Param.	incre.	GFLOPs	incre.	mIoU
HRNetV2	HRNetV2-W18	3.92M		71.6		76.2/75.9( <i>impl</i> )
Ours	GSTO-HRNet-W18	3.95M	▲0.67%	74.4	▲3.9%	<b>77.3</b> (1.1/1.4 ↑)
HRNetV2	HRNetV2-W48	65.78M		696.2		80.9/80.2( <i>impl</i> )
Ours	GSTO-HRNet-W48	65.93M	▲0.23%	714.0	▲2.6%	<b>82.1</b> (1.2/1.9 ↑)

Table 4: The increments of parameters and GFLOPs from HRNetV2 to our GSTO-HRNet and the mIoU comparison on Cityscapes val. (single scale and no flipping, not using OHEM during training).

	use val.	OHEM	MS	mIoU
HRNetV2-W48	✗	✗	✓	80.4
Ours-W48	✗	✗	✓	<b>81.9</b> (1.5 ↑)
HRNetV2-W48	✓	✗	✓	81.5
Ours-W48	✓	✗	✓	<b>82.3</b> (0.8 ↑)
HRNetV2-W48	✓	✓	✓	81.6
Ours-W48	✓	✓	✓	<b>82.4</b> (0.8 ↑)

Table 5: Comparison between HRNetV2 and GSTO-HRNet on Cityscapes test. *use val.* means using val. set for training and *MS* means Multi-scale testing.

Method	PPM	ASPP
Baseline	76.5	74.9
Baseline(w/ sup)	76.9(0.4 ↑)	75.1(0.2 ↑)
Baseline+GSTO(w/o sup)	77.3(0.8 ↑)	76.3(1.4 ↑)
Baseline+GSTO(w/ sup)	77.8(1.3 ↑)	76.9(2.0 ↑)

Table 6: Improvement on multi-scale aggregation modules.

	Backbone	#Param.	GFLOPs	mIoU
UNet++ [55]	ResNet-101	59.5M	748.5	75.5
DeepLabv3 [5]	Dilated-ResNet-101	58.0M	1778.7	78.5
DeepLabv3+ [7]	Dilated-Xception-71	43.5M	1444.6	79.6
PSPNet [52]	Dilated-ResNet-101	65.9M	2017.6	79.7
ACFNet[50]	ResNet-101	-	-	80.1
SPGNet[9]	2×ResNet-50	59.8M	654.8	80.9
HRNetV2[40]	HRNetV2-W48	65.8M	696.2	80.9
Our approach	GSTO-HRNet-W48	65.9M	714.0	<b>82.1</b>

Table 7: Comparison of semantic segmentation results on Cityscapes `val`. (single scale and no flipping, not using OHEM during training). The GFLOPs is calculated on the input size  $1024 \times 2048$ .

Method	Backbone	mIoU	iIoU cla.	IoU cat.	iIoU cat.
<i>Model learned on the train set</i>					
PSPNet [52]	Dilated-ResNet-101	78.4	56.7	90.6	78.6
PSANet [53]	Dilated-ResNet-101	78.6	-	-	-
PAN [21]	Dilated-ResNet-101	78.6	-	-	-
AAF [18]	Dilated-ResNet-101	79.1	-	-	-
HRNetV2[40]	HRNetV2-W48	80.4	59.2	91.5	80.8
ACFNet[50]	ResNet-101	80.8	-	-	-
Our approach	GSTO-HRNet-W48	<b>81.8</b>	<b>62.3</b>	<b>92.1</b>	<b>81.7</b>
<i>Model learned on the train+valid set</i>					
GridNet [14]	-	69.5	44.1	87.9	71.1
DeepLab [5]	Dilated-ResNet-101	70.4	42.6	86.4	67.7
FRRN [36]	-	71.8	45.5	88.9	75.1
RefineNet [24]	ResNet-101	73.6	47.2	87.9	70.6
DepthSeg [20]	Dilated-ResNet-101	78.2	-	-	-
BiSeNet [48]	ResNet-101	78.9	-	-	-
DFN [49]	ResNet-101	79.3	-	-	-
PSANet [53]	Dilated-ResNet-101	80.1	-	-	-
DenseASPP [47]	WDenseNet-161	80.6	59.1	90.9	78.1
SPGNet[9]	2×ResNet-50	81.1	-	-	-
HRNetV2[40]	HRNetV2-W48	81.6	61.8	92.1	82.2
ACFNet[50]	ResNet-101	81.8	-	-	-
Our approach	GSTO-HRNet-W48	<b>82.4</b>	<b>63.8</b>	<b>92.4</b>	<b>83.3</b>

Table 8: Comparison with state-of-the-art segmentation results on Cityscapes `test`.

Method	Backbone	Extra.	Pixel acc.	Avg. acc.	mIoU
Attention+SSL [15]	VGG16	Pose	84.36	54.94	44.73
DeepLabV3+ [7]	Dilated-ResNet-101	-	84.09	55.62	44.80
MMAN [27]	Dilated-ResNet-101	-	-	-	46.81
SS-NAN [54]	ResNet-101	Pose	87.59	56.03	47.92
MuLA [31]	Hourglass	Pose	88.50	60.50	49.30
JPPNet [22]	Dilated-ResNet-101	Pose	86.39	62.32	51.37
CE2P [37]	Dilated-ResNet-101	Edge	87.37	63.20	53.10
HRNetV2[40]	HRNetV2-W48	N	88.21	67.43	55.90
Our approach	GSTO-HRNet-W48	N	<b>88.38</b>	<b>68.36</b>	<b>57.37</b>

Table 9: Semantic segmentation results on LIP.  $N$  denotes not using any extra information, e.g., pose or edge.

## 4. Experiment

### 4.1. Dataset

#### 4.1.1 Semantic Segmentation

*Cityscapes* [10]. Cityscapes is a large-scale dataset focusing on semantic understanding of urban street scenes, containing 5,000 pixel-level annotated scene images divided into 2,975/500/1,525 images for training, validation and testing, respectively. For pixel-level labeling, there are 30 classes annotated and 19 of them used for evaluation.

*LIP* [15]. LIP is an elaborately annotated human parsing dataset, which contains 50,462 images annotated with 20 categories (19 for human parts and 1 for background). There are 30,462 images for training and 10,000 for validation.

*Pascal Context* [28]. Pascal Context is a challenging scene parsing dataset, including 4,998 images for training and 5,105 for testing. There are 60 classes, 59 for semantic category and 1 for background. We have tested our model on both conditions whether or not to ignore the background (denoted as “59 classes” and “60 classes”, respectively).

#### 4.1.2 Pose Estimation

*COCO* [25]. We use the COCO `train2017` for training, which contains 57K images and 150K person instances, annotated with 17 keypoints. Then we evaluate our model on COCO `val2017` and `test-dev2017`.

### 4.2. Evaluation metric

#### 4.2.1 Semantic Segmentation

We report the result for semantic segmentation mainly on the IoU-based metrics. IoU (intersection-over-union) is calculated by  $TP/(TP + FP + FN)$ , where  $TP$ ,  $FP$  and  $FN$  are the numbers of true positive, false positive and false negative pixels, respectively. For standard evaluation, mIoU (mean of IoU among based on classes) is exploited.

#### 4.2.2 Pose Estimation

OKS-based mAP (AP for short) is used for human pose estimation. OKS (Object Keypoint Similarity) is calculated through an unnormalized Gaussian distribution and outputs a value between 0 and 1, representing the similarity between the prediction and ground truth. Following previous arts, we report the average precision on several cases including large objects ( $AP^L$ ), medium objects ( $AP^M$ ),  $OKS = 0.5$  ( $AP^{50}$ ),  $OKS = 0.75$  ( $AP^{75}$ ), mean of  $OKS = 0.50, 0.55, \dots, 0.95$ , and the mean of average recall score on  $OKS = 0.50, 0.55, \dots, 0.95$  (AR).

Method	Backbone	Input size	#Param	GFLOPs	Val						Test						
					AP	AP <sup>50</sup>	AP <sup>75</sup>	AP <sup>M</sup>	AP <sup>L</sup>	AR	AP	AP <sup>50</sup>	AP <sup>75</sup>	AP <sup>M</sup>	AP <sup>L</sup>	AR	
Bottom-up: keypoint detection and grouping																	
OpenPose [1]	—	—	—	—	—	—	—	—	—	—	—	61.8	84.9	67.5	57.1	68.2	66.5
Associate Embedding [29]	—	—	—	—	—	—	—	—	—	—	—	65.5	86.8	72.3	60.6	72.6	70.2
PersonLab [32]	—	—	—	—	—	—	—	—	—	—	—	68.7	89.0	75.4	64.1	75.5	75.4
MultiPoseNet [19]	—	—	—	—	—	—	—	—	—	—	—	69.6	86.3	76.6	65.0	76.3	73.5
Top-down: human detection and single-person keypoint detection																	
Mask-RCNN [16]	ResNet-50-FPN	—	—	—	—	—	—	—	—	—	—	63.1	87.3	68.7	57.8	71.4	—
G-RMI [33]	ResNet-101	353 × 257	—	—	—	—	—	—	—	—	—	64.9	85.5	71.3	62.3	70.0	69.7
Integral Pose Regression [41]	ResNet-101	256 × 256	45.0M	11.0	—	—	—	—	—	—	—	67.8	88.2	74.8	63.9	74.0	—
8-stage Hourglass [30]	8-stage Hourglass	256 × 192	25.1M	14.3	66.9	—	—	—	—	—	—	—	—	—	—	—	—
CPN [8]	ResNet-50	256 × 192	27.0M	6.20	68.6	—	—	—	—	—	—	—	—	—	—	—	—
RMPE [13]	PyraNet	320 × 256	28.1M	26.7	—	—	—	—	—	—	—	72.3	89.2	79.1	68.0	77.2	78.5
CFN [?]	ResNet-Inception	384 × 288	—	—	—	—	—	—	—	—	—	72.6	86.1	69.7	78.3	64.1	—
CPN (ensemble) [8]	ResNet-Inception	384 × 288	—	—	—	—	—	—	—	—	—	73.0	91.7	80.9	69.5	78.1	79.0
SimpleBaseline [46]	ResNet-152	256 × 192	68.6M	15.7	72.0	89.3	79.8	68.7	78.9	77.8	—	—	—	—	—	—	—
SimpleBaseline [46]	ResNet-152	384 × 288	68.6M	35.6	74.3	89.6	81.1	70.5	79.7	79.7	73.7	91.9	81.1	70.3	80.0	79.0	—
HRNet-W32[39]	HRNet-W32	384 × 288	28.5M	16.0	75.8	90.6	82.7	71.9	82.8	81.0	74.9	<b>92.5</b>	82.8	71.3	80.9	80.1	—
HRNet-W48[39]	HRNet-W48	384 × 288	63.6M	32.9	76.3	<b>90.8</b>	82.9	72.3	83.4	81.2	75.5	<b>92.5</b>	83.3	71.9	81.5	80.5	—
Our approach	GSTO-HRNet-W32	384 × 288	<u>29.6M</u>	<u>18.2</u>	<b>76.5</b>	90.6	<b>83.1</b>	<b>72.6</b>	<b>83.7</b>	<b>81.4</b>	75.5	92.4	83.2	<b>72.0</b>	81.5	<b>80.6</b>	—
Our approach	GSTO-HRNet-W48	384 × 288	66.0M	37.6	<b>76.7</b>	90.7	<b>83.0</b>	<b>72.8</b>	<b>83.8</b>	<b>81.6</b>	<b>75.8</b>	<b>92.5</b>	<b>83.4</b>	<b>72.3</b>	<b>81.8</b>	<b>80.9</b>	—

Table 10: Comparisons on the COCO validation and test sets for pose estimation.

Method	Backbone	mIoU (59 classes)	mIoU (60 classes)
FCN-8s [26]	VGG-16	-	35.1
BoxSup [11]	-	-	40.5
DeepLab-v2 [4]	Dilated-ResNet-101	-	45.7
RefineNet [24]	ResNet-152	-	47.3
PSPNet [52]	Dilated-ResNet-101	47.8	-
Ding et al. [12]	ResNet-101	51.6	-
EncNet [51]	Dilated-ResNet-101	52.6	-
HRNetV2[40]	HRNetV2-W48	54.0	48.3
Our approach	GSTO-HRNet-W48	<b>54.3</b>	<b>48.5</b>

Table 11: Semantic segmentation results on PASCAL-context. The methods are evaluated on 59 classes and 60 classes.

### 4.3. Implementation Details

#### 4.3.1 Semantic Segmentation.

We follow the training protocol in [40]. For data augmentation, random cropping ( $512 \times 1024$  for Cityscapes,  $473 \times 473$  for LIP and  $480 \times 480$  for Pascal Context), random scaling in the range of  $[0.5, 2]$  and random horizontal flipping are exploited. We use SGD with momentum of 0.9 and poly learning rate policy with the power of 0.9 for all the datasets. The base learning rate is set as 0.01 for Cityscapes, 0.007 for LIP and 0.004 for Pascal Context. Weight decay is set as 0.0005 for Cityscapes and LIP, and 0.0001 for Pascal Context. Besides, we train our models for 600 epochs on Cityscapes with batch size of 12, 150 epochs on LIP with batch size of 40 and 280 epochs on Pascal Context with batch size of 16.

#### 4.3.2 Pose Estimation.

Following [39], we resize the detected box to fixed size:  $384 \times 288$ . Random rotation in the range of  $[-45^\circ, 45^\circ]$ , random scale in the range of  $[0.65, 1.35]$  and flipping are exploited as augmentation. We use the Adam optimizer and the base learning rate is set as 0.001, reduced to 0.0001 and 0.00001 at the 170th and 200th epochs, respectively. The batch size is set 128 for GSTO-HRNet-W32 and 80 for GSTO-HRNet-W48.

### 4.4. Ablation Study

We evaluate the proposed GSTO on the strong multi-scale backbone HRNet and conduct experiments to compare different inserting strategies and locations. Unless explicitly noted, the baseline model in this section is HRNetV2-W18-Small-v2, the results are reported on the Cityscapes validation dataset and the GFLOPs are calculated on the input size of  $1024 \times 2048$ .

#### 4.4.1 GSTO-based modules

Firstly, we evaluate two GSTO-based modules: Gated Fusion Module (GFM) and Gated Transition Module (GTM). As described in Section 3.2, GFM is exploited after each block to adaptively fuses the multi-scale features from each branch, and GTM is exploited after each stage to adaptively generate a lower-resolution branch. As shown in Table 1, performing GFM and unsupervised GTM improves the baseline by 0.7% and 0.5% respectively, and by 0.9% when both of them are applied. When we combine GTM

with the auxiliary supervision as proposed in Section 3.2, the result booms to 77.0%. When cooperated with GFM, it achieves 1.3% enhancement compared with the baseline (75.9%  $\rightarrow$  77.2%). *Specially, we note that simply utilizing extra supervision can only gain 0.4% growth, indicating that the proposed supervised GSTO makes good use of auxiliary supervision.*

#### 4.4.2 Number and location of supervised GTM

we further explore the number and location to apply the supervised GTM. We set the baseline as HRNetV2 with GFM only. Table 2 shows that auxiliary supervision is useful, and when the number of supervised GTM increases from 1 to 2, the performance improves from 76.7% to 77.3%. But exploiting to all three stages leads to 0.1% drop, indicating that shallow layers lacking semantic information can be even harmful for conducting the generation of the spatial gate. Therefore, exploiting supervised GTM only in stage2 and stage3 is the best choice with limited extra parameters and FLOPs, and we name this model as GSTO-HRNet.

#### 4.4.3 Compare with other gating mechanisms

In this part, we compare the proposed GSTO with previous attention-based modules, demonstrating that GSTO is a more effective strategy to apply gating/attention mechanism into pixel-labeling networks. We conduct experiments to compare GSTO (spatial attention combined with scale-transfer operation) with other attention forms (channel attention) and other locations to plug into the modules (after each block or after each layer). The results (as shown in Table 10) demonstrate that spatial attention is much more effective than channel-wise for pixel-labeling tasks, and *combining with scale-transfer operations for multi-scale feature extraction is a better way to bring the superiority of gating/attention mechanism than directly utilizing it in the end.*

### 4.5. Results on baseline

As demonstrated, the proposed GSTO can be easily inserted into any multi-scale feature extraction modules or backbones. We evaluate our method on strong multi-scale backbone HRNet[40][39] for both semantic segmentation and pose estimation, and on typical multi-scale modules PPM[52] and ASPP[4] for semantic segmentation.

#### 4.5.1 Results on GSTO-HRNet

We compare the proposed GSTO-HRNet with the baseline model HRNet in the aspects of parameters, computational costs and accuracy on Cityscapes for semantic segmentation and COCO for human pose estimation.

For Semantic segmentation, as presented in Table 4, with extra parameters less than 1% (0.67% for HRNetV2-W18

and 0.23% for HRNetV2-W48) and GFLOPs less than 5% (3.9% for HRNetV2-W18 and 2.6% for HRNetV2-W48), our GSTO-HRNet booms the mIoU by a large margin (75.9%  $\rightarrow$  77.3% and 80.2%  $\rightarrow$  82.1%, respectively) on the Cityscapes validation set. While in Table 5, exhaustive experiments on Cityscapes test set are conducted to compare the performance of HRNet and our approach, and the results demonstrate the superiority of our GSTO-HRNet.

For human pose estimation results in Table 10, our GSTO-HRNet-W32 significantly enhances the baseline from 75.8% AP to 76.5% AP on COCO validation set, which even outperforms the HRNet-W48 by 0.2 points while saving 53% parameters and 45% GFLOPs. The proposed GSTO-HRNet-W48 further improves the AP to 76.7%.

#### 4.5.2 Results on Multi-scale Modules with GSTO

Besides multi-scale backbones, the proposed Gated Scale-Transfer Operation can also improve general multi-scale modules by simply replacing conventional scale-transfer operation with GSTO. We verify this on the Cityscapes validation dataset for semantic segmentation in Table 6. The backbone is set as ResNet-50. It shows that supervised GSTO advances PPM by 1.3 points (76.5%  $\rightarrow$  77.8%) and advances ASPP by 2.0 points (74.9%  $\rightarrow$  76.9%).

### 4.6. Comparison with state-of-the-art

The proposed GSTO-HRNet achieves new state-of-the-art results on multiple benchmarks for pixel labeling tasks.

For semantic segmentation, GSTO-HRNet achieves 81.8% mIoU on Cityscapes test set using **only fine-labeled** train set and 82.4% using **only fine-labeled** train-val set (Table 8), which is the highest performance without using extra data like *Mapillary* and *COCO*. Besides, on the human parsing dataset LIP, GSTO-HRNet improves the state-of-the-art method by 1.5% on mIoU (Table 9), and on the complex scene parsing dataset Pascal Context, it again achieves best performance on both 59 classes and 60 classes (Table 11).

For pose estimation, we use the same person detector and tracking strategy as [39]. As shown in Table 10, performed on challenging COCO dataset without using any extra training data, our approach reaches state-of-the-art AP 76.7% on the validation set and 75.8% on the test set. Impressively, GSTO-HRNet achieves state-of-the-art result on the validation set (76.5%), outperforming the original HRNet-W48 with less parameters and smaller computational cost.

## 5. Further Visualization

Figure 1 has illustrated the visual comparison of the multi-scale features extracted by the encoder of HRNetV2-W48 (as the baseline) and the proposed GSTO-HRNet-



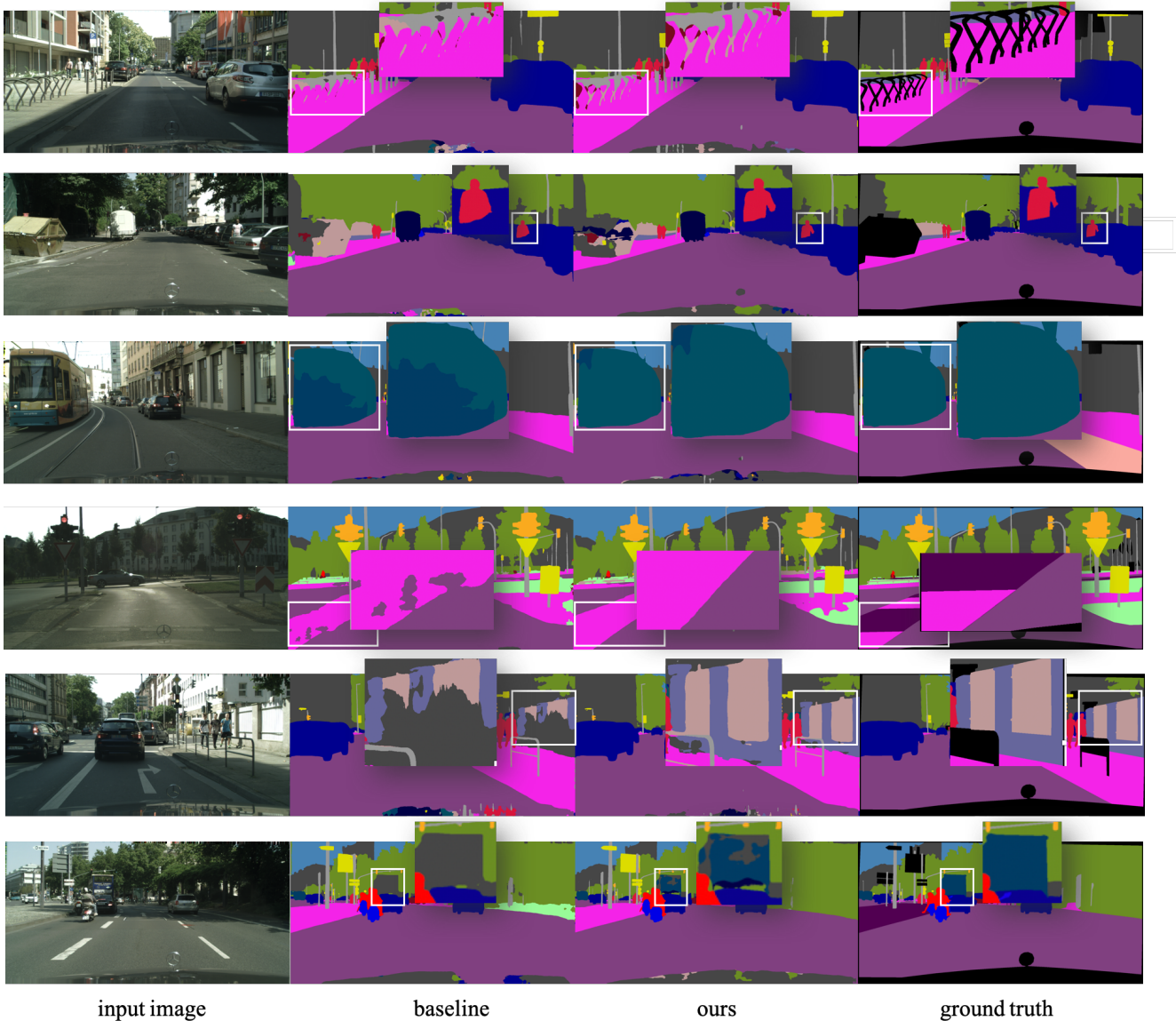


Figure 5: Example segmentation results of our method GSTO-HRNet-W48 and baseline HRNetV2-W48.

W48. In this section, we further provide the qualitative comparisons of segmentation results in Figure 5.

It indicates that our method captures more accurate boundary details than baseline model, like the road rail in the first instance and the leg of the person in the second row. Besides, the proposed GSTO keeps a consistency on large objects, like the "sidewalk" in the third instance, and the huge "train" in the fourth instance. Moreover, our method clearly obtains better semantic comprehension, since in the fifth example, the baseline method can hardly distinct the "fence", "wall" and "building", while our method achieves much better result. And in the last row, the occluded "bus"

can be easily confused with "truck", for which our model also performs better.

## 6. Conclusion

In this paper, we have proposed two forms of Gated Scale-Transfer Operations (GSTOs) for extracting more discriminative and scale-aware multi-scale features in pixel labeling. Experiments show that GSTOs significantly boost the multi-scale backbone HRNet and multi-scale modules like PPM and ASPP, with negligible extra parameters and computational cost. Moreover, the GSTO-based architecture GSTO-HRNet achieves new state-of-the-art results on

Cityscapes, LIP and Pascal Context datasets for semantic segmentation, and COCO for pose estimation.

## References

- [1] Zhe Cao, Tomas Simon, Shih-En Wei, and Yaser Sheikh. Realtime multi-person 2d pose estimation using part affinity fields. In *2017 IEEE Conference on Computer Vision and Pattern Recognition, CVPR 2017, Honolulu, HI, USA, July 21-26, 2017*, pages 1302–1310. IEEE Computer Society, 2017. 7
- [2] Liang-Chieh Chen, Yukun Zhu, George Papandreou, Florian Schroff, and Hartwig Adam. Encoder-decoder with atrous separable convolution for semantic image segmentation. In Vittorio Ferrari, Martial Hebert, Cristian Sminchisescu, and Yair Weiss, editors, *Computer Vision - ECCV 2018 - 15th European Conference, Munich, Germany, September 8-14, 2018, Proceedings, Part VII*, volume 11211 of *Lecture Notes in Computer Science*, pages 833–851. Springer, 2018. 3
- [3] Liang-Chieh Chen, George Papandreou, Iasonas Kokkinos, Kevin Murphy, and Alan L Yuille. Semantic image segmentation with deep convolutional nets and fully connected crfs. *arXiv preprint arXiv:1412.7062*, 2014. 1
- [4] Liang-Chieh Chen, George Papandreou, Iasonas Kokkinos, Kevin Murphy, and Alan L Yuille. Deeplab: Semantic image segmentation with deep convolutional nets, atrous convolution, and fully connected crfs. *PAMI*, 2018. 2, 3, 5, 7, 8
- [5] Liang-Chieh Chen, George Papandreou, Florian Schroff, and Hartwig Adam. Rethinking atrous convolution for semantic image segmentation. *arXiv:1706.05587*, 2017. 3, 6
- [6] Liang-Chieh Chen, Yi Yang, Jiang Wang, Wei Xu, and Alan L Yuille. Attention to scale: Scale-aware semantic image segmentation. In *CVPR*, 2016. 3
- [7] Liang-Chieh Chen, Yukun Zhu, George Papandreou, Florian Schroff, and Hartwig Adam. Encoder-decoder with atrous separable convolution for semantic image segmentation. In *ECCV*, 2018. 6
- [8] Yilun Chen, Zhicheng Wang, Yuxiang Peng, Zhiqiang Zhang, Gang Yu, and Jian Sun. Cascaded pyramid network for multi-person pose estimation. In *CVPR*, 2018. 7
- [9] Bowen Cheng, Liang-Chieh Chen, Yunchao Wei, Yukun Zhu, Zilong Huang, Jinjun Xiong, Thomas S. Huang, Wen-Mei Hwu, and Honghui Shi. Spgnet: Semantic prediction guidance for scene parsing. In *ICCV*, 2019. 3, 6
- [10] Marius Cordts, Mohamed Omran, Sebastian Ramos, Timo Rehfeld, Markus Enzweiler, Rodrigo Benenson, Uwe Franke, Stefan Roth, and Bernt Schiele. The cityscapes dataset for semantic urban scene understanding. In *CVPR*, 2016. 6
- [11] Jifeng Dai, Kaiming He, and Jian Sun. Boxesup: Exploiting bounding boxes to supervise convolutional networks for semantic segmentation. In *CVPR*, 2015. 7
- [12] Henghui Ding, Xudong Jiang, Bing Shuai, Ai Qun Liu, and Gang Wang. Context contrasted feature and gated multi-scale aggregation for scene segmentation. In *CVPR*, 2018. 7
- [13] Haoshu Fang, Shuqin Xie, Yu-Wing Tai, and Cewu Lu. RMPE: regional multi-person pose estimation. In *IEEE International Conference on Computer Vision, ICCV 2017, Venice, Italy, October 22-29, 2017*, pages 2353–2362. IEEE Computer Society, 2017. 7
- [14] Damien Fourure, Rémi Emonet, Elisa Fromont, Damien Muselet, Alain Tremeau, and Christian Wolf. Residual conv-deconv grid network for semantic segmentation. 2017. 6
- [15] Ke Gong, Xiaodan Liang, Dongyu Zhang, Xiaohui Shen, and Liang Lin. Look into person: Self-supervised structure-sensitive learning and a new benchmark for human parsing. In *CVPR*, 2017. 6
- [16] Kaiming He, Georgia Gkioxari, Piotr Dollár, and Ross B. Girshick. Mask R-CNN. In *IEEE International Conference on Computer Vision, ICCV 2017, Venice, Italy, October 22-29, 2017*, pages 2980–2988. IEEE Computer Society, 2017. 7
- [17] Jie Hu, Li Shen, and Gang Sun. Squeeze-and-excitation networks. In *CVPR*, 2018. 3
- [18] Tsung-Wei Ke, Jyh-Jing Hwang, Ziwei Liu, and Stella X. Yu. Adaptive affinity fields for semantic segmentation. In *ECCV*, 2018. 6
- [19] Muhammed Kocabas, Salih Karagoz, and Emre Akbas. Multiposenet: Fast multi-person pose estimation using pose residual network. In Vittorio Ferrari, Martial Hebert, Cristian Sminchisescu, and Yair Weiss, editors, *Computer Vision - ECCV 2018 - 15th European Conference, Munich, Germany, September 8-14, 2018, Proceedings, Part XI*, volume 11215 of *Lecture Notes in Computer Science*, pages 437–453. Springer, 2018. 7
- [20] Shu Kong and Charless C Fowlkes. Recurrent scene parsing with perspective understanding in the loop. In *CVPR*, 2018. 6
- [21] Hanchao Li, Pengfei Xiong, Jie An, and Lingxue Wang. Pyramid attention network for semantic segmentation. 2018. 6
- [22] Xiaodan Liang, Ke Gong, Xiaohui Shen, and Liang Lin. Look into person: Joint body parsing & pose estimation network and a new benchmark. *IEEE transactions on pattern analysis and machine intelligence*, 2018. 6
- [23] Guosheng Lin, Anton Milan, Chunhua Shen, and Ian D. Reid. Refinenet: Multi-path refinement networks for high-resolution semantic segmentation. In *2017 IEEE Conference on Computer Vision and Pattern Recognition, CVPR 2017, Honolulu, HI, USA, July 21-26, 2017*, pages 5168–5177. IEEE Computer Society, 2017. 3
- [24] Guosheng Lin, Anton Milan, Chunhua Shen, and Ian D Reid. Refinenet: Multi-path refinement networks for high-resolution semantic segmentation. In *CVPR*, 2017. 6, 7
- [25] Tsung-Yi Lin, Michael Maire, Serge Belongie, James Hays, Pietro Perona, Deva Ramanan, Piotr Dollár, and C Lawrence Zitnick. Microsoft coco: Common objects in context. In *ECCV*, 2014. 6
- [26] Jonathan Long, Evan Shelhamer, and Trevor Darrell. Fully convolutional networks for semantic segmentation. In *CVPR*, 2015. 7

- [27] Yawei Luo, Zhedong Zheng, Liang Zheng, Tao Guan, Junqing Yu, and Yi Yang. Macro-micro adversarial network for human parsing. In *ECCV*, 2018. 6
- [28] Roozbeh Mottaghi, Xianjie Chen, Xiaobai Liu, Nam-Gyu Cho, Seong-Whan Lee, Sanja Fidler, Raquel Urtasun, and Alan Yuille. The role of context for object detection and semantic segmentation in the wild. In *CVPR*, 2014. 6
- [29] Alejandro Newell, Zhiao Huang, and Jia Deng. Associative embedding: End-to-end learning for joint detection and grouping. In Isabelle Guyon, Ulrike von Luxburg, Samy Bengio, Hanna M. Wallach, Rob Fergus, S. V. N. Vishwanathan, and Roman Garnett, editors, *Advances in Neural Information Processing Systems 30: Annual Conference on Neural Information Processing Systems 2017, 4-9 December 2017, Long Beach, CA, USA*, pages 2277–2287, 2017. 7
- [30] Alejandro Newell, Kaiyu Yang, and Jia Deng. Stacked hourglass networks for human pose estimation. In *ECCV*. Springer, 2016. 3, 7
- [31] Xuecheng Nie, Jiashi Feng, and Shuicheng Yan. Mutual learning to adapt for joint human parsing and pose estimation. In *ECCV*, 2018. 6
- [32] George Papandreou, Tyler Zhu, Liang-Chieh Chen, Spyros Gidaris, Jonathan Tompson, and Kevin Murphy. Personlab: Person pose estimation and instance segmentation with a bottom-up, part-based, geometric embedding model. In Vittorio Ferrari, Martial Hebert, Cristian Sminchisescu, and Yair Weiss, editors, *Computer Vision - ECCV 2018 - 15th European Conference, Munich, Germany, September 8-14, 2018, Proceedings, Part XIV*, volume 11218 of *Lecture Notes in Computer Science*, pages 282–299. Springer, 2018. 7
- [33] George Papandreou, Tyler Zhu, Nori Kanazawa, Alexander Toshev, Jonathan Tompson, Chris Bregler, and Kevin Murphy. Towards accurate multi-person pose estimation in the wild. In *2017 IEEE Conference on Computer Vision and Pattern Recognition, CVPR 2017, Honolulu, HI, USA, July 21-26, 2017*, pages 3711–3719. IEEE Computer Society, 2017. 7
- [34] Jongchan Park, Sanghyun Woo, Joon-Young Lee, and In So Kweon. BAM: bottleneck attention module. In *British Machine Vision Conference 2018, BMVC 2018, Newcastle, UK, September 3-6, 2018*, page 147. BMVA Press, 2018. 3
- [35] Chao Peng, Xiangyu Zhang, Gang Yu, Guiming Luo, and Jian Sun. Large kernel matters—improve semantic segmentation by global convolutional network. In *CVPR*, 2017. 1, 3
- [36] Tobias Pohlen, Alexander Hermans, Markus Mathias, and Bastian Leibe. Full-resolution residual networks for semantic segmentation in street scenes. In *CVPR*, 2017. 3, 6
- [37] Tao Ruan, Ting Liu, Zilong Huang, Yunchao Wei, Shikui Wei, and Yao Zhao. Devil in the details: Towards accurate single and multiple human parsing. In *AAAI*, 2019. 6
- [38] Wenzhe Shi, Jose Caballero, Ferenc Huszár, Johannes Totz, Andrew P Aitken, Rob Bishop, Daniel Rueckert, and Zehan Wang. Real-time single image and video super-resolution using an efficient sub-pixel convolutional neural network. In *CVPR*, 2016. 3
- [39] Ke Sun, Bin Xiao, Dong Liu, and Jingdong Wang. Deep high-resolution representation learning for human pose estimation. 2019. 2, 3, 4, 5, 7, 8
- [40] Ke Sun, Yang Zhao, Borui Jiang, Tianheng Cheng, Bin Xiao, Dong Liu, Yadong Mu, Xinggang Wang, Wenyu Liu, and Jingdong Wang. High-resolution representations for labeling pixels and regions. *arXiv:1904.04514*, 2019. 1, 2, 3, 4, 5, 6, 7, 8
- [41] Xiao Sun, Bin Xiao, Fangyin Wei, Shuang Liang, and Yichen Wei. Integral human pose regression. In Vittorio Ferrari, Martial Hebert, Cristian Sminchisescu, and Yair Weiss, editors, *Computer Vision - ECCV 2018 - 15th European Conference, Munich, Germany, September 8-14, 2018, Proceedings, Part VI*, volume 11210 of *Lecture Notes in Computer Science*, pages 536–553. Springer, 2018. 7
- [42] Towaki Takikawa, David Acuna, Varun Jampani, and Sanja Fidler. Gated-scnn: Gated shape cnns for semantic segmentation. In *2019 IEEE/CVF International Conference on Computer Vision, ICCV 2019, Seoul, Korea (South), October 27 - November 2, 2019*, pages 5228–5237. IEEE, 2019. 3
- [43] Zhi Tian, Tong He, Chunhua Shen, and Youliang Yan. Decoders matter for semantic segmentation: Data-dependent decoding enables flexible feature aggregation. In *CVPR*, 2019. 3
- [44] Fei Wang, Mengqing Jiang, Chen Qian, Shuo Yang, Cheng Li, Honggang Zhang, Xiaogang Wang, and Xiaoou Tang. Residual attention network for image classification. In *2017 IEEE Conference on Computer Vision and Pattern Recognition, CVPR 2017, Honolulu, HI, USA, July 21-26, 2017*, pages 6450–6458. IEEE Computer Society, 2017. 3
- [45] Sanghyun Woo, Jongchan Park, Joon-Young Lee, and In So Kweon. Cbam: Convolutional block attention module. In *ECCV*, 2018. 3
- [46] Bin Xiao, Haiping Wu, and Yichen Wei. Simple baselines for human pose estimation and tracking. In *ECCV*, 2018. 7
- [47] Maoke Yang, Kun Yu, Chi Zhang, Zhiwei Li, and Kuiyuan Yang. Denseaspp for semantic segmentation in street scenes. In *CVPR*, 2018. 3, 6
- [48] Changqian Yu, Jingbo Wang, Chao Peng, Changxin Gao, Gang Yu, and Nong Sang. Bisenet: Bilateral segmentation network for real-time semantic segmentation. *ECCV*, 2018. 6
- [49] Changqian Yu, Jingbo Wang, Chao Peng, Changxin Gao, Gang Yu, and Nong Sang. Learning a discriminative feature network for semantic segmentation. In *CVPR*, 2018. 6
- [50] Fan Zhang, Yanqin Chen, Zhihang Li, Zhibin Hong, Jingtuo Liu, Feifei Ma, Junyu Han, and Errui Ding. Acfnnet: Attentional class feature network for semantic segmentation. In *ICCV*, 2019. 6
- [51] Hang Zhang, Kristin Dana, Jianping Shi, Zhongyue Zhang, Xiaogang Wang, Amrith Tyagi, and Amit Agrawal. Context encoding for semantic segmentation. In *CVPR*, 2018. 7
- [52] Hengshuang Zhao, Jianping Shi, Xiaojuan Qi, Xiaogang Wang, and Jiaya Jia. Pyramid scene parsing network. In *CVPR*, 2017. 2, 3, 5, 6, 7, 8

- [53] Hengshuang Zhao, Zhang Yi, Liu Shu, Shi Jianping, Chen Change Loy, Lin Dahua, and Jiaya Jia. Psanet: Point-wise spatial attention network for scene parsing. *ECCV*, 2018. 6
- [54] Jian Zhao, Jianshu Li, Xuecheng Nie, Fang Zhao, Yunpeng Chen, Zhecan Wang, Jiashi Feng, and Shuicheng Yan. Self-supervised neural aggregation networks for human parsing. In *CVPRW*, 2017. 6
- [55] Zongwei Zhou, Md Mahfuzur Rahman Siddiquee, Nima Tajbakhsh, and Jianming Liang. Unet++: A nested u-net architecture for medical image segmentation. In *MICCAI*. Springer, 2018. 6